Supporting Information

Sakaba et al. 10.1073/pnas.1219234110

SI Materials and Methods

Immunohistochemistry. Mice were killed by an overdose of ketamin/rompun (10 μL/10 g body weight given i.p.) and transcardially perfused with 50 mL of saline solution [0.85% NaCl, 0.025% KCl, and 0.02% $NaHCO_3$ (pH 6.9), with 0.01% heparin, at body temperature], followed by 50 mL of cold (7–15 °C), freshly depolymerized 4% paraformaldehyde (PFA; Merck) in 0.1 M PBS (pH 7.4). Brains were carefully removed from the skulls, postfixed overnight in the same fixative, and placed in a mixture of 20% glycerol and 2% dimethyl sulfoxide (VWR International) in 0.4 M PBS for 24 h, for cryoprotection. Frozen coronal sections of brainstem containing medial nucleus of the trapezoid body (MNTB) were cut to 15-μm thickness using a sliding microtome.

For immunostaining, sections were first washed in PBS (three washes, 15 min each), then washed in PBS containing 0.3% Triton-X-100 (nine washes, 20 min each) and preincubated with PBS containing 5% normal goat serum and 0.3% Triton X-100 for 1 h. Incubation with primary antibodies was performed for 48 h at 4 °C. Mouse monoclonal bassoon antibody (1:600 dilution, SAP 7F407; Abcam) and rabbit polyclonal intersectin 1 antibody (1:250) (1) were diluted in PBS containing 0.3% Triton-X-100. Localization of dynamin at the active zone (AZ) was done using mouse monoclonal dynamin antibody (1:100, Hudy1; Upstate Biotechnology) and rabbit polyclonal piccolo antibody (1:200, Synaptic Systems), both diluted as above. Next, the sections were washed nine times for 20 min each in 0.3% Triton-X-100 in 0.1 M PBS, then incubated with secondary antibodies labeled with ATTO 647N (1:200; ATTO-TEC) and Chromeo 494 (1:200; Active Motif) for 12 h using standard techniques. Finally, sections were mounted on gelatin-coated glass slides and embedded by a gradual exchange of PBS with 2,2-thiodiethanol in PBS, resulting in an embedding medium of 97% (vol/vol) 2.2-thiodiethanol in PBS.

For intersectin 1 SH3A injections, a patch pipette was used to inject the mixture of ATTO 647N-conjugated SH3A domain and Alexa Fluor 488 into the presynaptic terminal. After a few minutes of dialysis, the patch pipette was retracted to maintain a functionally intact terminal. The slice was then fixed in 4% PFA, subsequently embedded in a gelatin/albumin mixture (4.8% gelatin from porcine kin, type A, G 2500; Sigma-Aldrich and 12% albumin from chicken egg white, grade II, A 5253; Sigma-Aldrich) in demineralized water, oriented horizontally, and postfixed overnight in 10% PFA in 0.1 PBS at 4 °C. Calyxes were then resectioned into 15-μm-thick sections with a vibrating-blade microtome (VT 1000S; Leica) and immunostained as described above. The immunostainings shown in Fig. S2 were performed in two couples each of WT and intersectin 1 KOs using quinea pig polyclonal VGLUT1 antibody (1:500, Synaptic Systems) and mouse monoclonal AP2 antibody (1:200, AP6, Abcam). The secondary antibodies were highly cross-absorbed Alexa 488 goat anti-gunea pig (1:400) and Alexa 568 goat anti-mouse (1:400), respectively. Four WT/ intersectin 1 KO couples were used for immunoblot analyses.

Stimulated Emission Depletion and Confocal Imaging. Confocal and stimulated emission depletion (STED) images were acquired on a Leica TCS dual-color STED microscope equipped with an inverted microscope (DMI 6000; Leica) and a 100 × STED objective (HCX PL APO 100×, 1.4 NA oil STED). ATTO 647N and Chromeo 494 were excited using pulsed-diode lasers (<90 ps, 80 MHz) at 635 nm and 531 nm, respectively. Stimulated emission depletion was achieved using a Ti:Sapphire laser tuned to 750 nm and ∼300-ps pulses. For optimal STED efficiency, the STED beam pulse was delayed relative to the synchronized diode lasers (delay time, ∼8,200 ps fpr ATTO 647N, ∼7,954 ps for Chromeo 494). Dual-color emission was separated by a dichroic mirror (BS 650 nm), and emission was detected through bandpass filters (BP 582/75 for Chromeo 494 and BP 685/40 for ATTO 647N). STED images were acquired at a 60-Hz scan rate (lines/s) with 4× line averaging and a zoom factor of 6, resulting in a 25-nm pixel size. The alignment between STED and the excitation beam was routinely controlled.

The width of fluorescence peaks at half-maximum values were ∼300 nm in confocal mode and ∼100–150 nm for the same image captured in STED mode, providing a measure of the increase in resolution with STED imaging. Single STED *x-y* images of AZs were acquired after adjusting the focus of the 100× objective in the confocal mode to the fluorescence maximum of an object of interest. To quantitatively determine the degree of colocalization between bassoon and intersectin 1 clusters, we calculated the Pearson's correlation coefficient (*Rr*) from confocal images. To exclude the possibility of random colocalization we repeated the analysis after shifting the red (intersectin 1) image over a distance of 10 pixels (approximately corresponding to the size of a single AZ) relative to the green (bassoon) image (Fig. S1, see also Fig. 1 for color code).

1. Pechstein A, et al. (2010) Regulation of synaptic vesicle recycling by complex formation between intersectin 1 and the clathrin adaptor complex AP2. *Proc Natl Acad Sci USA* 107(9):4206–4211.

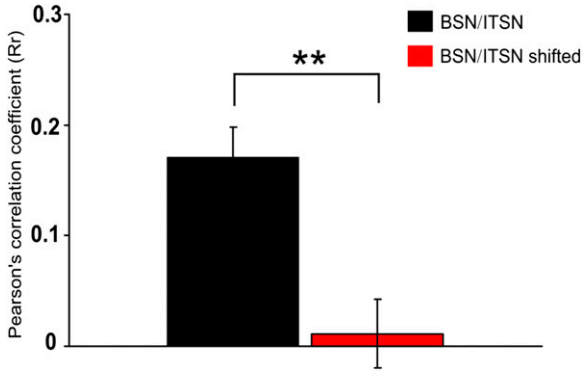

Fig. S1. Partial but nonrandom colocalization of intersectin 1 and bassoon clusters at the calyx of Held. Pearson's correlation coefficient of $Rr = 0.171 \pm 0.027$ (black bar) indicates a partial colocalization of bassoon (BSN) and intersectin 1 (ITSN1) clusters. To exclude the possibility of random colocalization we repeated the analysis after shifting the red (ITSN1) channel over a distance of 10 pixels (approximately corresponding to the size of a single AZ) relative to the green (BSN) channel. The *Rr* value calculated from shifted images (red bar) was significantly lower ($Rr = 0.0114 \pm 0.031$) compared with nonshifted images ($P < 0.006$) indicating partial but nonrandom colocalization of BSN and ITSN1 clusters.

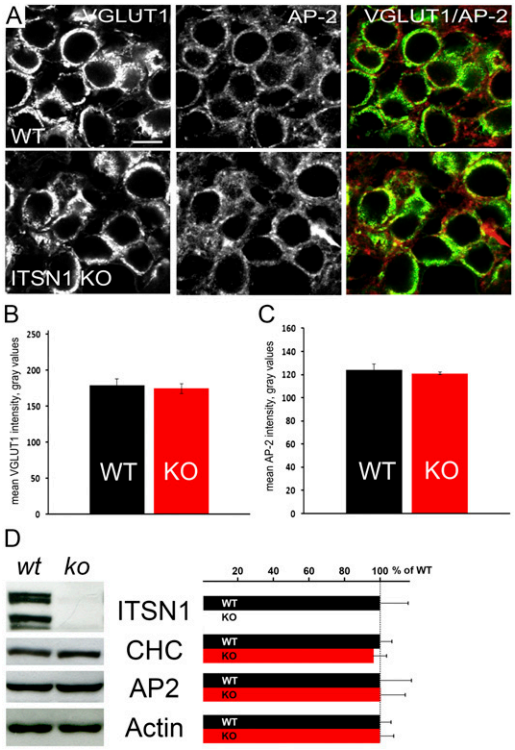

Fig. S2. Levels of clathrin and AP-2 in intersectin 1 KO mice. (*A*) Confocal microscopy images of calyx of Held synapses from WT (*Upper*) and intersectin 1 (ITSN1) KO (*Lower*) mice immunostained for endogenous vesicular glutamate transporter 1 (VGLUT-1) and adaptor protein complex 2 (AP-2). Note that the morphology of calyces in the absence of ITSN1 is preserved. The intensity of VGLUT-1, a major component of synaptic vesicles (SVs) at excitatory synapses, is unaltered. (Scale bar: 10 μm.) (*B* and *C*) Mean fluorescent intensity of VGLUT-1 (*B*) and AP-2 (*C*) in the calyx of Held from WT (black bars) and ITSN1 KO (red bars) mice ($n = 2$). Fluorescent intensity of AP-2 was quantified in VGLUT1-positive regions of interest. (*D*) Levels of clathrin heavy chain (CHC) and AP-2 in lysates derived from the MNTB area of brainstems derived from WT and ITSN1 KO mice (P10–P11, littermates) were probed by immunoblotting with the indicated antibodies. Signal intensities from WT samples were taken as 100%.

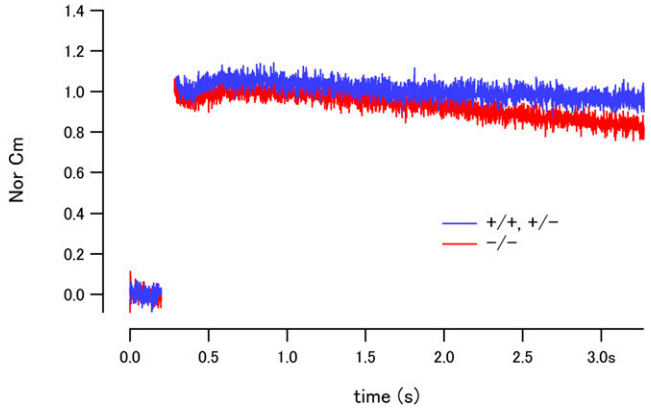

Fig. S3. Fast capacitance measurements following a depolarizing pulse in intersectin KO mice. The same data as shown in Fig. 2*D* (50-ms pulse), but capacitance was monitored at a faster time scale after stimulation. In each cell, the capacitance trace was normalized to the peak value. Data from $^{+/+}$ (WT) or $^{+/-}$ (heterzygotes) are in blue (n = 6 cells); that from $^{-/-}$ (KO) are in red (n = 6 cells). Error bars are omitted for clarity. No significant differences among these conditions were seen. During the pulse, it was impossible to measure capacitance, owing to large conductance changes. Because fast endocytosis was not seen in our recording conditions, it is unlikely that replenishment of FRP is linked to kiss-and-run events in our conditions. The lack of difference between WT and KO indicates that membrane retrieval per se does not regulate SV replenishment.

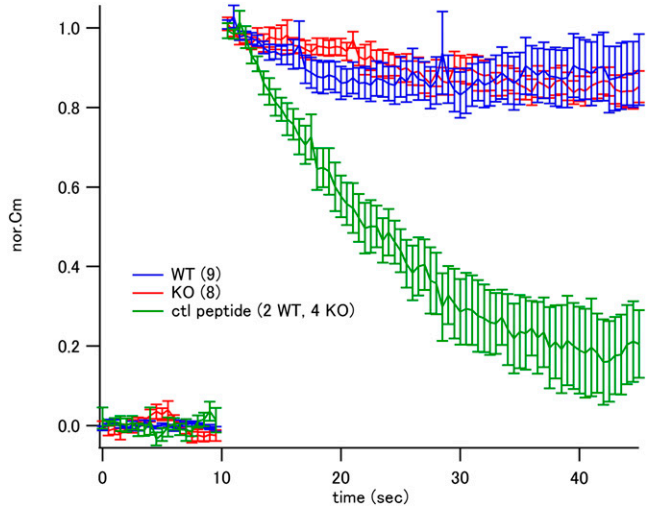

Fig. S4. Interference with AP2 function blocks endocytic membrane retrieval in WT and intersectin 1 KO mice. In this set of experiments, presynaptic capacitance was measured to monitor exocytosis and endocytosis. The presynaptic terminal was depolarized from −80 mV to +70 mV for 2 ms and then repolarized to 0 mV for 50 ms (Fig. 2). The patch pipette contained 100 μM Syt2 peptide (KRLKKKKTTVKK) to block clathrin-mediated endocytosis (1). In both WT and KO, endocytosis after the depolarizing pulse was blocked. Capacitance jumps were similar in WT and KO (WT, 242 ± 29 fF; KO, 208 ± 33 fF), indicating that blocking AP2 function does not induce fast endocytosis during the pulse. A mutant control peptide unable to bind to AP2 (ARLEADKTTVAD; two WT cells and four KO cells) was ineffective. Thus, WT and KO cells respond similarly to perturbation of clathrin/AP2-mediated endocytosis. Postsynaptic responses were also measured in this set of experiments. A pair of depolarizing pulses (0 mV for 50 ms after a prepulse to +70 mV for 2 ms) was applied to the presynaptic terminal with an interval of 500 ms. Monitoring of recovery of the FRP showed that only 3% ± 3% was recovered during the second pulse in WT (n = 6), and 5% ± 5% was recovered in KO (n = 6). Therefore, the peptide blocked both endocytosis and SV replenishment.

1. Hosoi N, Holt M, Sakaba T (2009) Calcium dependence of exo- and endocytotic coupling at a glutamatergic synapse. *Neuron* 63(2):216–229.

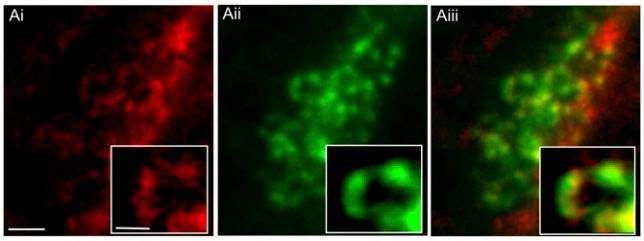

Fig. S5. Dynamin localization at the calyx of Held revealed by STED microscopy. STED image of a calyx of Held synaptic terminal immunostained for endogenous dynamin 1/2 (*i*; red) and piccolo (*ii*; green), an AZ marker. Two images are overlaid in *iii*. (*Insets*) Dynamin 1/2-immunopositive puncta outlining single AZs. (Scale bars: 800 nm; 350 nm in *Insets*). Dynamin and piccolo fluorescence overlap partially (yellow in *iii*), indicating that dynamin partially localizes to AZs. The majority of dynamin 1/2 is seen within the surrounding periactive zone, consistent with its known role in endocytosis.

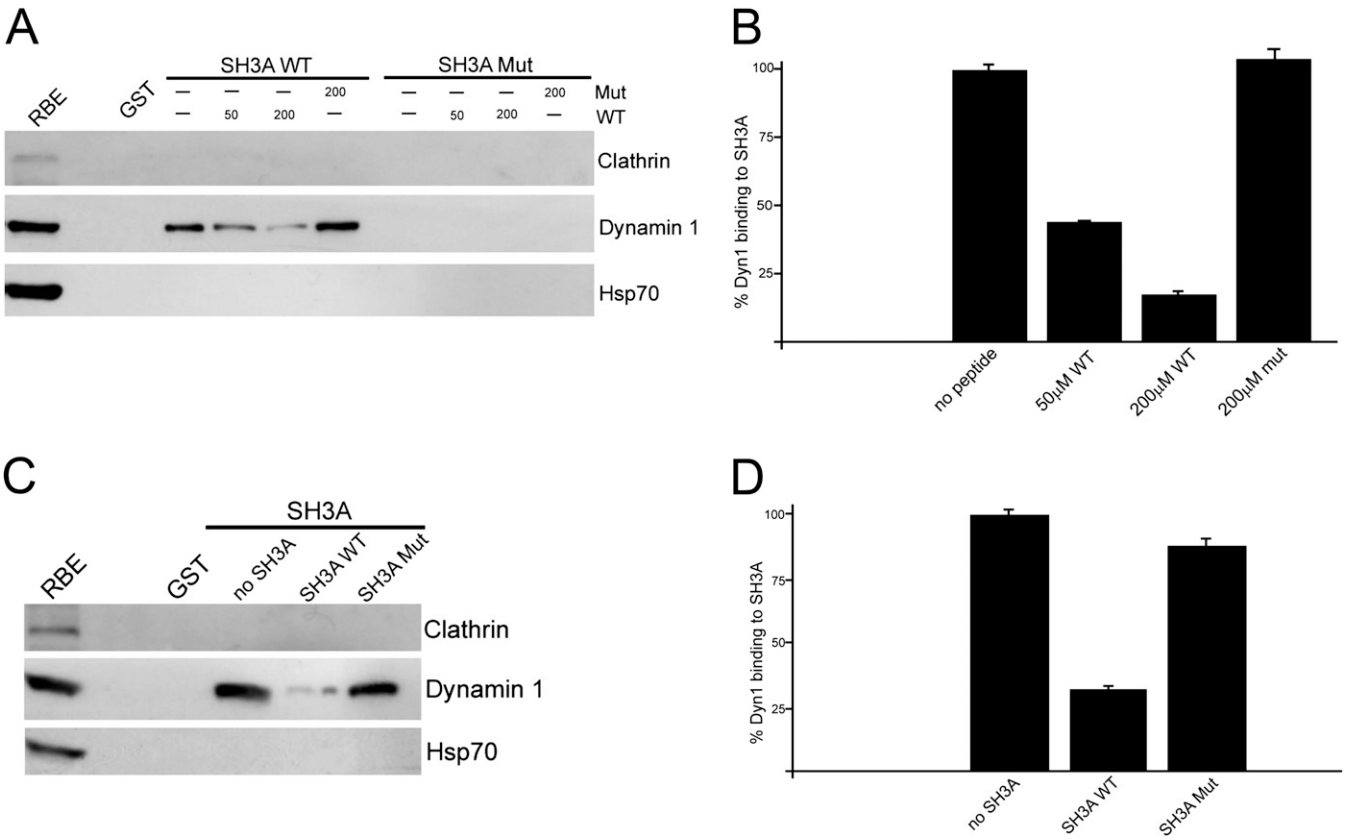

Fig. S6. Competition of intersectin 1–dynamin 1 complex formation by dynamin 1-derived proline-rich peptide or the SH3A domain of intersectin 1. (*A*) Affinity isolation of intersectin 1 SH3A domain binding proteins from rat brain extract (RBE) in the presence of a dynamin 1-derived proline-rich peptide. First, 20 μg of GST-ITSN1 SH3A WT or G794R, P797L (GPRL) mutant (Mut) were incubated with RBE (1 mg/mL) in the presence of 50 μM or 200 μM dynamin 1-derived proline-rich peptide (WT) or an inactive mutant (Mut) thereof. Samples were analyzed by SDS/PAGE and immunoblotting against dynamin 1 or clathrin heavy chain and heat-shock cognate protein of 70 kD (Hsc70) as negative controls. (*B*) Quantification of data shown in *A* ($n = 2$ independent experiments). The amount of dynamin 1 bound to GST-SH3A in the absence of peptide was taken as a 100%. (*C*) Affinity isolation of intersectin 1 SH3A domain binding proteins from RBE (1 mg/mL) in the presence of hexahistidine (His_6)-ITSN SH3A (WT) or an inactive GPRL mutant thereof (Mut). First, 20 μg of GST-ITSN1 SH3A was incubated with RBE in the presence of 20 μM His6-ITSN1 SH3A (WT) or with the inactive GPRL mutant (Mut). Samples were analyzed by SDS/PAGE and immunoblotting against dynamin 1 or clathrin heavy chain and Hsc70 as negative controls. (*D*) Quantification of data shown in C in two independent experiments. The amount of dynamin 1 bound to GST-SH3A in the absence of added protein was taken as a 100%.

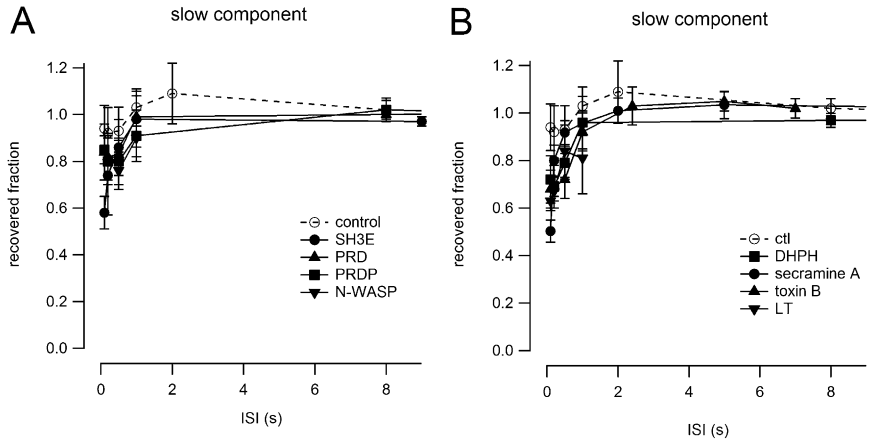

Fig. S7. Recovery of the slowly releasing component. The data were obtained from the experiments shown in Figs. 4 and 5. A pair of depolarizing pulses (depolarization to +70 mV for 2 ms, followed by repolarization to 0 mV for 50 ms) was applied with different intervals, and recovery of the slowly releasing component (SRP) was monitored. (*A*) Control data (open circles), in the presence of SH3E (filled circles), the dynamin proline-rich domain (filled triangles), a peptide derived from the proline-rich domain of dynamin (filled squares) or the proline-rich domain of *N*-WASP (filled inverse triangles). (*B*) Control recordings (open circles), the data in the presence of the DH-PH domain of intersectin 1 (filled squares), secramine A (filled circles), toxin B (filled triangles), or lethal toxin (filled inverse triangles). Minor differences from the control data were noticed at the interval of 0.1 s, but the effect was miniscule compared with recovery of the fast component. Moreover, in previous studies, recovery of the slow component at the 0.1-s interval was somewhat variable and ranged between 70% and 90%.

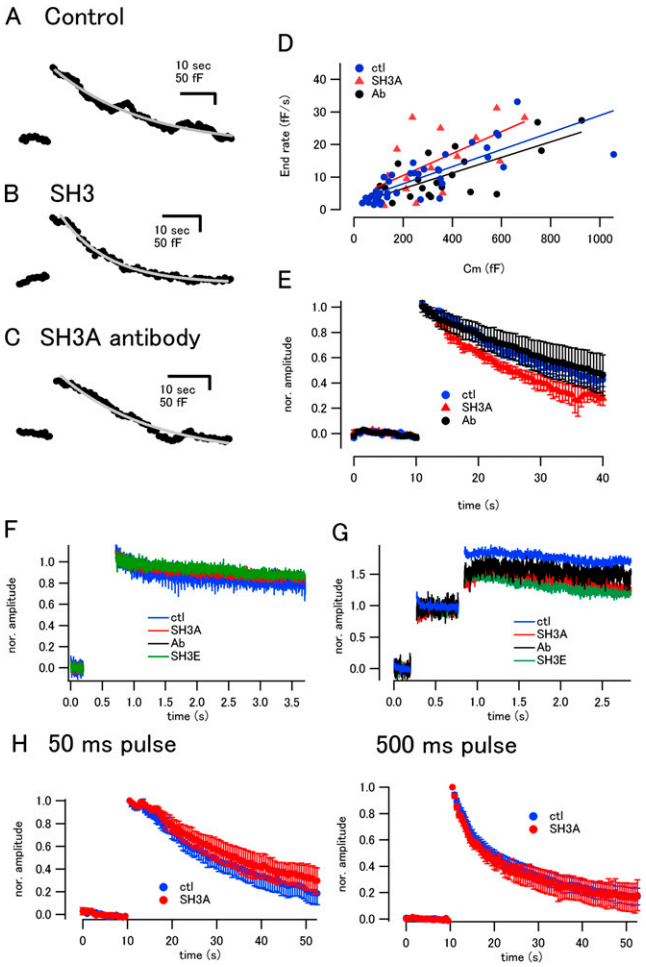

Fig. S8. Analysis of the capacitance decay. (*A–F*) In this set of experiments, a train of AP-like stimulations (depolarization to +40 mV for 1 ms at 100 Hz) was applied to the presynaptic terminal in the presence of 0.1 mM EGTA within the patch pipette. The number of pulses was varied to elicit different amounts of exocytosis, and capacitance traces were recorded. In response to stimulation, jumps in membrane capacitance were observed, reflecting exocytosis. After these exocytic jumps, the membrane capacitance decayed back to baseline with time constants of tens of seconds corresponding to endocytic membrane retrieval, consistent with previous studies at the calyx synapse. The data were fitted by a single exponential (gray traces in *A–C*). If a line fit was more appropriate, then the capacitance decay was fitted by a line. The rate of endocytosis was calculated by dividing the peak capacitance jump by the time constant or using a slope from the line fitted in *D*. Blue, red, and black circles represent the control data and the data in the presence of intersectin SH3A domain and antibody, respectively. There is no difference among the three conditions. (*E*) Average time course of capacitance decay in response to a train of AP-like stimuli (100 Hz for 20 or 50 pulses) plotted against time. In each cell, the capacitance trace was normalized to the peak value. Data from control conditions (blue circles, $n = 9$ cells), in the presence of SH3A (red triangles, $n = 4$ cells), or antibodies against intersectin 1-SH3A domain (black circles, $n = 4$ cells) are shown. No statistical differences were observed among these conditions. (*F*) Capacitance was monitored at a faster time scale after stimulation. In each cell, the capacitance trace was normalized to the peak value. Error bars are omitted. (*G*) Capacitance measured with fast time resolution. A depolarizing pulse (depolarization to +70 mV for 2 ms, followed by repolarzation to 50 ms) was applied twice with an interval of 500 ms. Capacitance was monitored concurrently to assess the rate of endocytosis immediately after the pulse. A 50-ms pulse depletes the entire RRP (FRP + SRP). In *F* and *G*, blue, red, black, and green traces indicate the data under control, in the presence of SH3A domain, or antibodies against the SH3A or SH3E domains of intersectin 1, respectively. The data were normalized to the capacitance jump after the first 50-ms pulse. Error bars are omitted for clarity. The time courses of capacitance changes due to endocytic membrane retrieval were unchanged in the presence of intersectin 1-perturbing reagents (SH3A domain, antibodies against the SH3A or SH3E domains). (*H*) Presynaptic patch pipettes contained 0.5 mM EGTA. The presynaptic terminal was depolarized from −80 mV to +70 mV for 2 ms, and then repolarized to 0 mV for either 50 ms (*Left*) or 500 ms (*Right*). Blue and red traces represent data from the control condition and the condition in the presence of intersectin SH3A domain, respectively. The time course of endocytosis was normalized to the peak amplitude. As shown, there were no differences between the two conditions.

Table S1. Time course of release during a depolarizing pulse

Condition	*n*	Calcium current (I_{Ca}), pA	Fast tau, ms	Slow tau, ms	Fraction (fast, %)
Control	5	1,529 ± 45	1.4 ± 0.2	15.9 ± 1.7	49 ± 4
ITSN1 SH3A	8	1,072 ± 37	1.9 ± 0.3	14.1 ± 2.3	56 ± 5
SH3A antibody	5	1,239 ± 107	2.4 ± 0.4	18.5 ± 3.2	58 ± 3
SH3A GPRL	5	1,445 ± 125	1.8 ± 0.2	16.4 ± 1.9	42 ± 5
Endophilin 1A SH3	3	1,364 ± 122	1.8 ± 0.3	21.5 ± 7.6	52 ± 5
ITSN1 SH3E	7	1,433 ± 133	2.4 ± 0.7	19.0 ± 3.6	53 ± 4
Dynamin1 proline-rich domain (PRD)	5	1,124 ± 83	3.2 ± 0.6	25.3 ± 3.4	40 ± 4
Dynamin1 PRD peptide	4	1,153 ± 85	2.1 ± 0.7	22.0 ± 5.4	55 ± 4
N-WASP PRD	3	1,009 ± 149	3.8 ± 0.4	33.3 ± 6.1	50 ± 3
ITSN1 Dbl homology-pleckstrin homology domain (DH-PH)	6	1,257 ± 158	2.7 ± 0.5	19.5 ± 3.4	45 ± 4
Dynamin1 PRD peptide	4	1,153 ± 85	2.1 ± 0.7	22.0 ± 5.4	55 ± 4
ITSN1 DHPH	6	1,257 ± 158	2.7 ± 0.5	19.5 ± 3.4	45 ± 4
Secramine A	8	1,276 ± 185	2.6 ± 0.2	34.2 ± 3.9	54 ± 3
Toxin B	7	1,412 ± 59	2.6 ± 0.4	29.3 ± 5.1	59 ± 4
Lethal toxin	5	1,054 ± 24	2.5 ± 0.4	22.9 ± 4.4	51 ± 2

The data were obtained from Figs. 4 and 5. Presynaptic patch pipettes contained 0.5 mM EGTA. The presynaptic terminal was depolarized from −80 mV to +70 mV for 2 ms, followed by repolarization to 0 mV for 50 ms. During a 50-ms pulse, the RRP (fast and slow components, FRP and SRP) is depleted. The time course of cumulative release was fitted by a double-exponential fit. In previous studies, the amplitudes of presynaptic calcium currents were ~1,000–1,500 pA, the time constant of the fast component of release was 1–3 ms, the time constant of the slow component of release was 10–30 ms, and the fraction of the fast component was 40–60%. Thus, the values presented here are within the range of previously reported results. Although Ca currents were slightly smaller in the presence of reagents, these differences did not change the recovery of FRP.